Astron. Astrophys. 283, 677–692 (1994)

ASTRONOMY AND ASTROPHYSICS

Turbulent accretion disk dynamos

Ulf Torkelsson[1] **and Axel Brandenburg**[2,3]

[1] Lund Observatory, Box 43, S-221 00 Lund, Sweden
[2] HAO/NCAR*, P.O. Box 3000, Boulder, CO 80307, USA
[3] NORDITA, Blegdamsvej 17, DK-2100 Copenhagen Ø, Denmark

Received 12 May 1993 / Accepted 11 September 1993

Abstract. We present numerical results for mean-field $\alpha^2\Omega$-dynamos in an accretion disk. We first study the linear case in both disks with constant thickness and disks with radially increasing thickness. The preferred mode is dipolar for a thick disk, but quadrupolar for a thin one. The quadrupolar mode generates a magnetic torque that transports angular momentum outwards. The rôle of the geometrical distribution of both the α-effect and the magnetic diffusivity in the disk is considered for thin disks. It is found that the parity of the most easily excited mode is unaffected, albeit the distribution of the magnetic field and torque change in such a way that a larger fraction of the field and the torque appears in regions with small diffusivity. For some interesting cases we study nonlinear effects like α-quenching and magnetic buoyancy. These effects can affect significantly the magnetic field distribution, compared to the linear case. A transition to chaotic behaviour is found for α-quenching when α is negative in the upper part of the disk.

Key words: accretion: accretion disks – (MHD) – novae, cataclysmic variables – galaxies: active – galaxies: jets – turbulence

1. Introduction

The rôle of magnetic fields in accretion disks is still largely unknown, but they possess a great potential for important effects (e.g. Blandford 1989), such as driving the accretion through the magnetic torque on the disk and collimating outflowing material to a jet. There is a growing body of observational facts indicating the presence of magnetohydrodynamic processes in accretion disks. Some of the most interesting examples are the radio outbursts of Cyg X-3 and 3C 120 (Shields & Wheeler 1976), the magnetism of meteorites (Levy 1978) and the behaviour of Balmer emission in cataclysmic variables (Horne & Saar 1991), which are described in more detail below.

Send offprint requests to: Ulf Torkelsson

* The National Center for Atmospheric Research is sponsored by the National Science Foundation

The most direct probes of the protosolar nebulae are surviving primordial material like comets and carbonaceous chondrites. Levy (1978) notes that carbonaceous chondrites are normally permanently magnetised. As they seem to be unprocessed remnants of the primordial solar nebulae, there must have been a magnetic field in that part of the solar nebula, where the carbonaceous chondrites formed. This magnetic field could have been sustained by a dynamo. A counter argument against this hypothesis has been that most of the solar nebula was cold and neutral. However Levy (1978) argues that it could have been ionised by the radioactive decay of ^{26}Al. Another possible ionising agent is cosmic rays, and Stepinski (1992) shows that this may in fact be a more efficient way of ionising the solar nebulae.

Shields & Wheeler (1976) discuss two ways of generating radio outbursts. Firstly, they look at how much magnetic energy that can be stored in an accretion disk while still being consistent with the magnetic field acting as a source of viscosity in the disk. For reasonable physical parameters they show that the total energy released in the outbursts of 3C 120 can be stored in the accretion disk, but that this is not possible for Cyg X-3. Secondly, they look at the rate of generation of magnetic energy by the winding up of the field lines due to the differential rotation of the accretion disk, and compare this with an estimate of the rate of release of energy during the outburst. They find that in the outbursts of both 3C 120 and Cyg X-3 magnetic energy could be regenerated at the same rate as energy is released. Thus magnetic flares are a possible explanation for the radio outbursts in these objects.

Strong observational evidence for dynamo action in accretion disks comes from the study of the strength of emission lines from the accretion disks of cataclysmic variables by Horne & Saar (1991). They have mapped the strength of Balmer emission, Hβ, in accretion disks by using Doppler tomography (e.g. Marsh & Horne 1990). Their results show that the variation of the strength of the Balmer line emission along the disk radius is proportional to the Keplerian angular velocity. This should be compared to the well known fact that emission lines indicative of chromospheric activity in stars, primarily Ca II H and K, but also the Balmer lines, have line strengths proportional to the stellar angular velocity (e.g. Skumanich 1972, Noyes et al.

1984). Unfortunately no maps of disks in Ca II H and K have been presented so far, due to that these lines are blended with adjacent Balmer lines.

All the facts mentioned above emphasise the importance of improving our understanding of the processes creating the magnetic fields in accretion disks and the distribution of the field in the disk. The common approach to describe the production of magnetic fields in stars with outer convection zones is the mean-field dynamo (e.g. Krause & Rädler 1980). The idea behind the mean-field formalism is to express the magnetic and velocity fields as the sum of an averaged field and a fluctuating field. In this way the induction equation can be split into two coupled equations describing, respectively, the evolution of the mean and the fluctuating magnetic field. There is an additional term in the mean-field equation resulting from the correlation between the fluctuating magnetic and velocity fields. This term represents both the generation as well as the destruction of the mean magnetic field due to the turbulent motions, i.e. the α-effect and the turbulent magnetic diffusivity. It is thus possible to calculate the mean magnetic field with only a limited knowledge of the fluctuating fields.

This concept has been extended to galaxies in order to explain the observed magnetic fields of spiral galaxies (e.g. Parker 1971, Stix 1975, Rosner & DeLuca 1989). The first attempts at modelling a dynamo in an accretion disk were made by Takahara (1979) and Pudritz (1981). These early investigations were purely analytical, and the first numerical calculations were carried out by Stepinski & Levy (1988, 1990b, hereafter referred to as SL88 and SL90, respectively) who solved an eigenvalue problem. Numerical calculations have also been carried out by Camenzind (1991) using a time-stepping method based upon a finite element method. Time-stepping methods have the general advantage of being suitable for nonlinear dynamos.

In this paper we present numerical computations of a mean-field dynamo acting in an accretion disk. Our method and the basic features of our model are presented in Sect. 2. The results of our code are compared with the work of SL88 and SL90 in Sect. 3. In Sect. 4 we study the effect of changing the disk geometry, and thus determine the importance of the geometrical distribution of the α-effect and the magnetic diffusivity on the magnetic field. Sect. 5 explores the nonlinear quenching and the effect of magnetic buoyancy on the dynamo. Both the effects of changing the geometrical distribution of the induction effects as well as nonlinearity have not fully been explored in previous work. Finally, Sect. 6 is devoted to a discussion of the results.

2. Governing equations and numerical methods

2.1. The dynamo equation

The evolution of the mean magnetic field is described by the induction equation

$$\frac{\partial \boldsymbol{B}}{\partial t} = \boldsymbol{\nabla} \times (\boldsymbol{u} \times \boldsymbol{B} + \alpha \boldsymbol{B} - \eta_t \mu_0 \boldsymbol{J}), \quad \boldsymbol{\nabla} \cdot \boldsymbol{B} = 0, \tag{1}$$

where $\boldsymbol{u}$ is the mean field velocity, α the parameter describing the isotropic effect of the turbulence on the magnetic field, (not to be confused with the α-parameter employed in the thin accretion disk theory of Shakura & Sunyaev 1973), η_t the turbulent magnetic diffusivity, μ_0 the magnetic permeability of free space, and $\boldsymbol{J} = \boldsymbol{\nabla} \times \boldsymbol{B}/\mu_0$ the electric current. We take $\boldsymbol{u} = \hat{\boldsymbol{\phi}} \varpi \Omega$, where ϖ is the distance from the axis, and Ω the angular velocity.

In the present paper we ignore the anisotropy of the α-tensor and the magnetic diffusivity, although it may be of importance (Rüdiger 1990), especially for the generation of nonaxisymmetric magnetic fields. In accretion disks differential rotation is relatively strong, which leads to a rapid winding up of nonaxisymmetric mean magnetic fields, and thus to their enhanced dissipation. Therefore the neglect of anisotropies and nonaxisymmetric field generation is partially justified.

As measures of the strength of the α-effect and the differential rotation we introduce the dynamo numbers

$$C_\alpha = \frac{\alpha_0 R}{\eta_{\rm disk}}, \tag{2}$$

and

$$C_\Omega = \frac{\Omega_0 R^2}{\eta_{\rm disk}}, \tag{3}$$

where α_0 is a typical value for α, R the outer radius of the disk, $\eta_{\rm disk}$ the magnetic diffusivity inside the disk at the radius R, and Ω_0 the maximum of the angular velocity in the disk.

The medium outside an accretion disk is usually believed to have a very low effective conductivity (e.g. SL88). This may best be modelled by adopting a vacuum boundary condition on the surface of the disk, which requires solving a Laplace equation for the potential of the magnetic field outside this surface. Since this is difficult in an arbitrary geometry we follow here the approach of embedding the disk into a sphere with lower conductivity, for which the vacuum boundary condition can easily be formulated. This method was first used by SL88 in the context of accretion disks. According to the standard theory for thin disks the turbulent velocity is much larger than the velocity of matter inflow. We will therefore neglect the radial velocity, even though the disks considered below cannot be regarded as thin. Note, however, that Rüdiger et al. (1993) included the effects of a magnetically induced accretion flow on the dynamo.

Eq. (1) is solved in spherical polar coordinates, r, θ, ϕ. The assumption of axisymmetry means that all quantities are independent of the azimuthal angle ϕ, but we allow toroidal magnetic and velocity fields. It is then advantageous to write $\boldsymbol{B} = b\hat{\boldsymbol{\phi}} + \boldsymbol{B}_{\rm p}$, where $\boldsymbol{B}_{\rm p} = \boldsymbol{\nabla} \times (a\hat{\boldsymbol{\phi}})$, and the subscript p denotes the poloidal component. The dynamo equation reduces then to two equations for a and b. In two dimensions, Eq. (1) can be written as

$$\left(\partial_t - \eta_t D^2\right) a = \alpha b \tag{4}$$

and

$$\left(\partial_t - \eta_t D^2\right) b = \alpha j + \hat{\boldsymbol{\phi}} \cdot \left[\boldsymbol{\nabla}\alpha \times \boldsymbol{B}_{\rm p} - \boldsymbol{\nabla}\eta_t \times \boldsymbol{J}_{\rm p}\right] + \varpi \boldsymbol{B}_{\rm p} \cdot \boldsymbol{\nabla}\Omega, \tag{5}$$

where $j = -D^2 a$ is the current density, and D^2 the Stokes operator with $D^2 a = -\hat{\phi} \cdot \nabla \times \nabla \times (a\hat{\phi})$. Dimensionless units are employed as defined below.

We solve Eqs. (4) and (5) using a time-stepping method described in more detail in Brandenburg et al. (1989). Unless stated otherwise we use a timestep of $5\ 10^{-6}$ magnetic diffusion time units, and a 41×41 or 41×81 grid for computations on one or two quadrants in the meridional plane, respectively.

2.2. Units

To make the variables dimensionless we choose the units

$$[r] = R,\ [t] = R^2/\eta_{\rm disk},\ [u] = \eta_{\rm disk}/R,$$
$$[B] = [u]\,(\mu_0 \rho_0)^{1/2}; \qquad (6)$$

where ρ_0 is the typical density in the disk at the radius R, and R is taken as approximately six times the inner radius of the disk, which will include the most strongly radiating parts of the disk. In order to get some feeling for the dimensions we give rough estimates for several types of objects surrounded by accretion disks: a magnetic neutron star (NS), a stellar mass black hole (SMBH), and the black hole in an active galactic nucleus (AGN). There is no separate entry for a white dwarf, because the disk of a moderately magnetic white dwarf would appear similar to the disk of the neutron star, even though the total amount of energy released will be much larger for the neutron star, as it is much smaller. These estimates are presented in Table 1, where we have assumed a standard thin accretion disk with the Shakura & Sunyaev (1973) viscosity parameter $\alpha_{\rm SS} = 0.1$. Several of the quantities given in Table 1 are directly accessible from the Shakura-Sunyaev model and were evaluated at radius R. An upper limit for the magnitude of the α-effect is $\alpha_0 \sim z_0 \Omega_0$, where z_0 is the half-thickness of the disk and Ω_0 the maximum angular velocity in the disk, assuming that the turbulent correlation length cannot be larger than z_0. By assuming that the magnetic Prandtl number is of order unity we can set the turbulent magnetic diffusivity $\eta_{\rm t}$ equal to the turbulent viscosity $\nu_{\rm t} = \alpha_{\rm SS} z_0 c_{\rm s}$ as given in the Shakura-Sunyaev model, where $c_{\rm s} = z_0 \Omega$ is the speed of sound. Finally we also give the ratio $\xi = z_0/R$ and the plasma $\beta = 2\mu_0 p/B^2$. Note that in order to simulate a vacuum surrounding the grid we have to choose $\eta_{\rm out}$ for the part of the grid outside the disk to be much larger than $\eta_{\rm disk}$ inside the disk.

The small dynamo numbers for the supermassive black hole in an AGN is due to our choice of a relatively modest mass for the black hole and a high accretion rate, which results in an accretion rate close to the Eddington limit, implying that the thin disk theory is invalid and the estimate strictly irrelevant. However we keep it as a warning against naively applying the theory of thin accretion disks, which will yield unrealistic results at too high accretion rates.

2.3. The disk model

We now specify the angular velocity, the α-effect and the magnetic diffusivity in the disk. The angular velocity is well known in the theory of thin accretion disks where one assumes that the disk is centrifugally supported in the radial direction. Here we adopt profiles for α and Ω that closely resemble those used by SL88. We will thus assume that the rotation is Keplerian in the outer parts of the disk, but that it turns over to rigid rotation in the innermost part of the disk in order to avoid a singularity in the angular velocity on the polar axis.

Table 1. Typical parameters for some accretion disks. The parameters for the AGN has been chosen to achieve an accretion rate close to the Eddington limit. In this case thin disk theory becomes invalid, and our formal estimates therefore unrealistic

Object	NS	SMBH	AGN
$M (M_\odot)$	1	10	10^7
R (m)	$2\,10^7$	$6\,10^5$	$6\,10^{11}$
$\dot{M}$ ($M_\odot$ yr^{-1})	10^{-9}	$2\,10^{-9}$	1
C_α	100	400	1
C_Ω	10^5	10^6	10
ξ	0.01	0.004	1
$\eta_{\rm disk}$ (m^{2}s^{-1})	10^{10}	$4\,10^8$	$3\,10^{19}$
$[t]$ (s)	40 000	900	10 000
$[u]$ (m s^{-1})	500	700	$6\,10^7$
ρ (kg m^{-3})	$2\,10^{-2}$	30	$3\,10^{-9}$
$[B]$ (T)	0.07	4	3
β	$2\,10^4$	10^6	$3\,10^{-6}$

$$\Omega(\varpi) = \Omega_0 \frac{R}{\varpi_0} \left(\frac{3}{2^{2/3}}\right)^{1/n} \left[1 + \left(\frac{\varpi}{\varpi_0}\right)^{3n/2}\right]^{-1/n}, \qquad (7)$$

where ϖ_0 is the distance from the rotational axis to the point where the rotation changes from being rigid to Keplerian, z the vertical coordinate, and z_0 the half-thickness of the disk. The index n should be large to provide a sharp transition from rigid to Keplerian rotation. In practice we put $n = 10$ as a compromise between a sharp turnover and numerical roundoff errors. Note that in most cases we set the angular velocity outside the disk to zero (in a similar fashion as for the α-effect below), which gives a strong vertical gradient in Ω at the disk surface. However, comparing solutions with and without rotation outside the disk, we do not find any significant differences in the resulting magnetic field. Note that in some of our calculations below the rigidly rotating part of the disk is replaced by an inner cavity which behaves as a vacuum.

It is harder to give expressions for the α-effect and the turbulent diffusivity, as these depend on the ill-known properties of turbulence in the disk. However some authors have tried to give qualitative estimates of the functional form of these quantities (e.g. Stepinski & Levy 1991). We use an α-effect of the same form as that used by SL88, SL90:

$$\alpha = \alpha_0 z \frac{\Omega}{\Omega_0} F(z), \qquad (8)$$

where

$$F(z) = [\Theta(z + z_0) - \Theta(z - z_0)], \qquad (9)$$

and Θ is the Heaviside step function which, in practice, is approximated by the continuous function $\frac{1}{2}[1+\tanh(z/d)]$, where $d = 0.2$.

For the first test cases we used a magnetic diffusivity given by

$$\eta_t = \eta_{\rm out} + (\eta_{\rm disk} - \eta_{\rm out})F(z), \tag{10}$$

where $\eta_{\rm out}/\eta_{\rm disk} = 10 - 50$. This is similar to SL88, but note that they used a ratio of 200, whereas we only could increase the ratio to 50 for a few test cases. Large diffusivity ratios are numerically expensive to handle, because of the wide range of time scales involved. Recent experiments showed however that a much larger diffusivity ratio can be handled if we force all induction effects (in particular the differential rotation) to be zero outside the disk.

3. Test cases

In this section we present critical dynamo numbers, i.e. the minimum values of $C_\alpha C_\Omega$ required for dynamo action, for pure parity modes for models that have previously been considered by SL88. SL88 also use spherical polar coordinates and their results, as well as ours of test calculations for constant η_t and $\alpha \propto \cos\theta$, are in perfect agreement with those of Roberts (1972). Hence, in the calculations presented in this section, we basically test the implementation of the disk structure in the model. We also present results for uniform disk thickness, which should be in qualitative agreement with those of SL90, who used a cylindrical geometry and a much thinner disk than we do.

Since the induction effects, differential rotation and α-effect, are either symmetric or antisymmetric about the equatorial plane, the marginal modes are also either symmetric (S0) or antisymmetric (A0) about this plane, where "0" denotes axisymmetry. Symmetric (antisymmetric) modes are referred to as quadrupolar (dipolar) modes. We will calculate the dynamo modes for both positive and negative C_α, although we only expect positive C_α to occur in real disks. The sign of C_α is indicated by + or − on the symbol for the mode.

3.1. Radially increasing disk thickness

The model calculated by SL88 was for a flared disk, i.e. with radially increasing thickness, described by

$$z_0(\varpi) = \zeta_0 + \zeta\varpi, \tag{11}$$

where $\zeta_0 = \zeta = 0.25$.

For this disk configuration we calculate the critical dynamo numbers for the lowest dipole and quadrupole modes. Those numbers are presented in Table 2. To check the importance of the angular velocity outside the disk we study two cases. In case I we keep the angular velocity constant on cylinders even outside the disk, whereas it was put to zero outside the disk in case II. We also give the angular frequency $\omega = 2\pi/T$ for oscillating modes in Table 2, where T is the period. The dynamo numbers and angular frequencies can be compared with the results of SL88, which are also given in Table 2. Note that we have taken the square of their dynamo numbers to get $C_\alpha C_\Omega$. The most striking difference between their results and ours is that the magnitude of their dynamo numbers are systematically larger than ours (compare columns I, II and SL88). This may be due to the fact that they were able to use a larger relative difference for the magnetic diffusivity. To check the importance of the magnetic diffusivity we increased the ratio $\eta_{\rm out}/\eta_{\rm disk}$ to 50 for case II, and calculated the lowest modes. These results are given as case III in Table 2. The results for the A0 mode with $C_\alpha C_\Omega < 0$ are now much closer to the corresponding numbers in SL88, but for the other modes the dynamo numbers become larger than the corresponding ones in SL88. We may also note from Table 2 that the discrepancies get marginally smaller for case II, which could be interpreted as this being a more truthful representation of a surrounding vacuum. On the other hand, we do not note any improvements for the angular frequencies. The remaining discrepancies might also result from a lower resolution in SL88 (20×20). The main conclusion from Table 2 is that the most easily excited mode is dipolar for $C_\alpha > 0$ and quadrupolar for $C_\alpha < 0$.

3.2. Magnetic field geometry for flared disks

Depending on the sign of the dynamo number $C_\alpha C_\Omega$ we obtain oscillatory solutions with field migration either towards the disk plane ($C_\alpha C_\Omega > 0$) or away from it ($C_\alpha C_\Omega < 0$). The vertical field migration is accompanied by an additional motion in the ϖ-direction: field belts moving towards the disk plane are pushed outwards before they fade away, whereas field belts moving away from the disk plane turn towards the axis before they disappear. The maximum of the toroidal field strength occurs at $\varpi \approx 0.3$, which is close to the position of the maximum shear. The field geometry of A0 and S0 solutions is roughly similar in most of the disk and there are differences only in the immediate vicinity of the disk plane.

The evolution of the magnetic field and torque for the most easily excited mode is displayed in Fig. 1. Note that the zero point in time has been chosen arbitrarily. The magnetic field can be compared to Fig. 2 in SL88 and the magnetic torque to Fig. 2 in Stepinski & Levy (1990a). The torque is given by

$$\tau = \varpi\hat{\boldsymbol{\phi}} \cdot (\boldsymbol{J} \times \boldsymbol{B}). \tag{12}$$

The agreement with their calculations is good. Notice the existence of regions with negative torque and that the magnitude of the negative torque is greater than that of the positive torque. This suggests that the magnetic torque can contribute to the transport of angular momentum and drive the accretion. However, one should keep in mind that the strength of the magnetic field and thus the strength of the torque is undetermined for a linear dynamo. The magnetic torque is concentrated to particular areas in the disk and so the accretion would be highly nonuniform. At this point we need to remember that the fluctuating part of the magnetic field should also be included. Given our limited knowledge of the torque exerted by this small scale

Table 2. Comparison of the critical dynamo numbers $C_\alpha C_\Omega$ and the angular frequencies ω for flared disks with $\zeta = \zeta_0 = 0.25$ and $\varpi_0 = 0.25$. The diffusivity ratio $\eta_{\rm out}/\eta_{\rm disk}$ is 20 in cases I and II, and 50 in case III. $C_\Omega = 100\eta_{\rm out}/\eta_{\rm disk}$. The angular velocity outside the disk is put to zero in cases II and III. The lowest critical dynamo numbers are printed in bold face

	$C_\alpha C_\Omega$				ω			
	I:	II	III	SL88	I	II	III	SL88
S0	24 000	25 000	33 000	29 000	390	410	480	390
A0	**16 000**	**17 000**	**22 000**	**19 000**	280	290	330	280
S0	**−27 000**	**−27 000**	**−38 000**	**−35 000**	590	600	650	560
A0	−29 000	−30 000	−40 000	−40 000	520	520	720	660

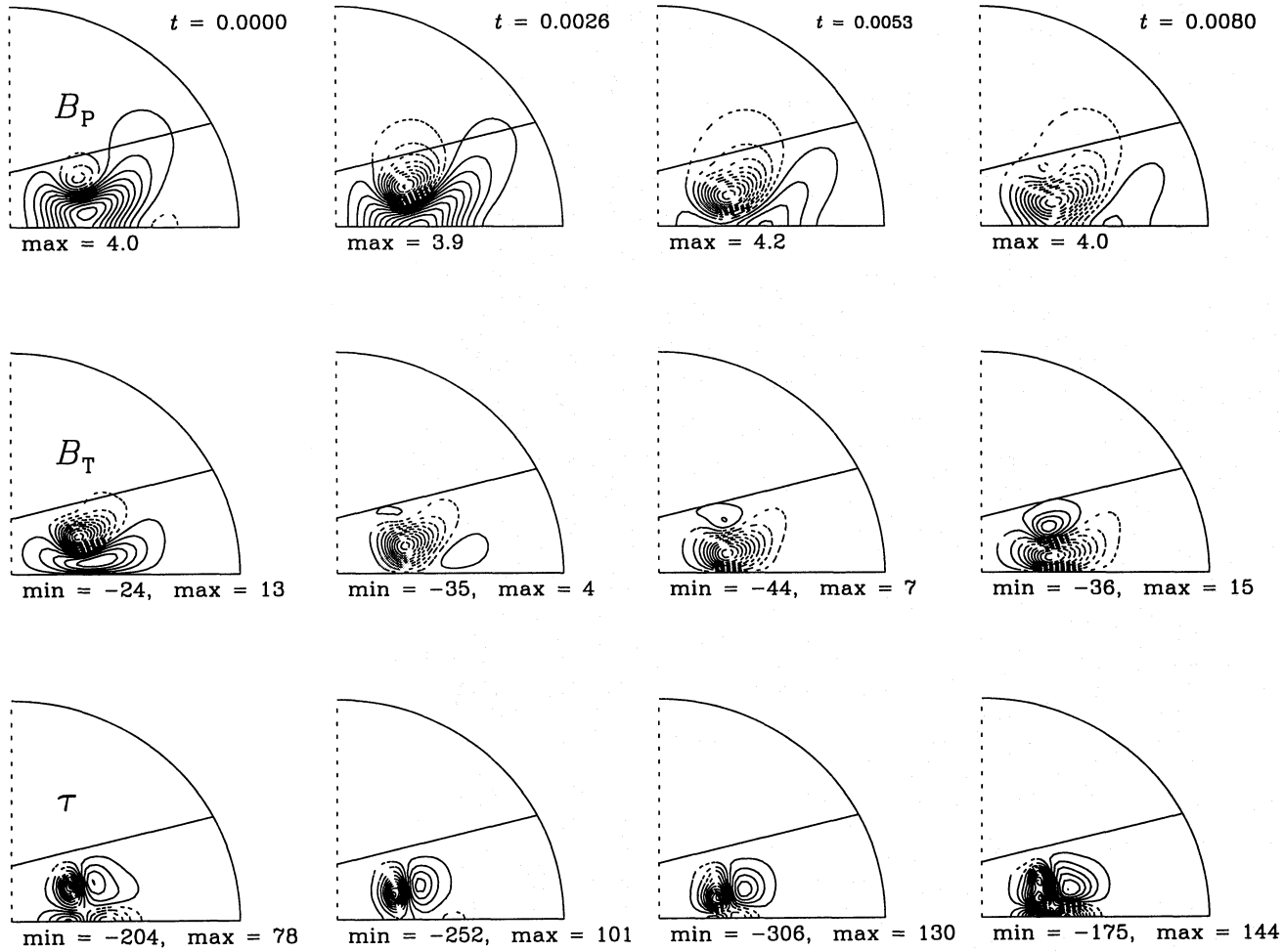

Fig. 1. The evolution of the most easily excited dynamo mode, A0$^+$, in a disk with $\zeta_0 = \zeta = 0.25$ and $\varpi_0 = 0.25$ during almost half a cycle period. The dynamo numbers are $C_\Omega = 2000$, $C_\alpha C_\Omega = 17000$, and the magnetic diffusivity $\eta_{\rm out}/\eta_{\rm disk} = 20$. In the upper row field lines of the poloidal field $B_{\rm p}$ are displayed. In the middle and last rows we show contours of the toroidal field $B_{\rm t}$ and the torque τ. The minima and maxima of the fields are given. For the poloidal magnetic field only the maximum strength is given. Solid contours mark positive values and dashed contours negative values. In the first row solid (dashed) contours denote clockwise (counterclockwise) orientation. The disk boundary is indicated by a solid line

field, one should consider the results for the torque due to the mean magnetic field alone with suitable caution.

3.3. Disks with uniform thickness

In Table 3 we present critical dynamo numbers for disks with constant thickness and $\varpi_0 = 0.25$. These numbers are given for $C_\Omega = 2000$ and 20000. Since $C_\alpha C_\Omega$ is not very different in these two cases we can deduce that we are in the $\alpha\Omega$-regime. There is perfect agreement between the dynamo numbers for the most easily excited mode in the two cases. For disks with uniform thickness SL90 calculated critical dynamo numbers using an $\alpha\Omega$-dynamo both for disks surrounded by a vacuum and disks surrounded by an electrically conducting medium. Their models were calculated in a cylindrical geometry imposing approximate boundary conditions in z, that allowed the disks to be thinner than we could achieve in our spherical geometry. Thus, we cannot make any quantitative comparison with SL90. However we may note that they also find that the easiest excited mode is $S0^+$. For a disk of relative thickness $h/r = 0.05$ and $\varpi_0/R = 0.05$ they obtain the critical dynamo number $C_\alpha C_\Omega = 81$. Note also the difference in the sign of the definition of the dynamo numbers, which is due to the minus sign on the right-hand-side of Eq. (7) in SL90.

An important difference between our model and the model employed by Stepinski and Levy is that their model has rigid rotation only in the innermost 5%. It would require a substantially larger grid resolution to have such a small zone with rigid rotation. Instead we calculated a sequence of models for $\varpi_0 = 0.25, 0.15$ and 0.1; see Fig 2. Because of numerical stability requirements we had to decrease the timestep for models with $\varpi_0 = 0.15$ and 0.1 to $2.5\,10^{-6}$ and $1.25\,10^{-6}$, respectively.

There seems to be some qualitative disagreements between our results and SL90, because SL90 obtain an oscillating $A0^-$ mode whilst we find a steady one. This is a result of the smaller value of ϖ_0. In Fig. 2 we display the critical dynamo numbers for the different modes as a function ϖ_0. For small values of ϖ_0 the $A0^-$-mode becomes oscillatory. Another discrepancy is that SL90 found it easier to excite a $S0^-$-mode than an $A0^-$-mode, while the reverse result is seen in Table 3. Figures 2 and 3 demonstrate that this too is an effect of the thinner disk with a smaller region of rigid rotation in SL90. Note that for the $z_0 = 0.15$ model in Fig. 3 we used a 63×64 grid and a timestep of $2.5\,10^{-6}$, otherwise we employed the same grid size as before, as tests with higher resolution did not show any significant differences. For an analytical approach to the determination of the disk modes see Soward (1992).

3.4. Magnetic field geometry for disks with uniform thickness

The field configuration of the most easily excited dynamo mode for a disk with $\varpi_0 = 0.15$ and $z_0 = 0.2$ is displayed in Fig. 4. As this is a steady dynamo it is sufficient to display the magnetic field at one time. Note the simple topology of the quadrupole-type field and the strong concentration of the negative magnetic torque to the inner part of the accretion disk.

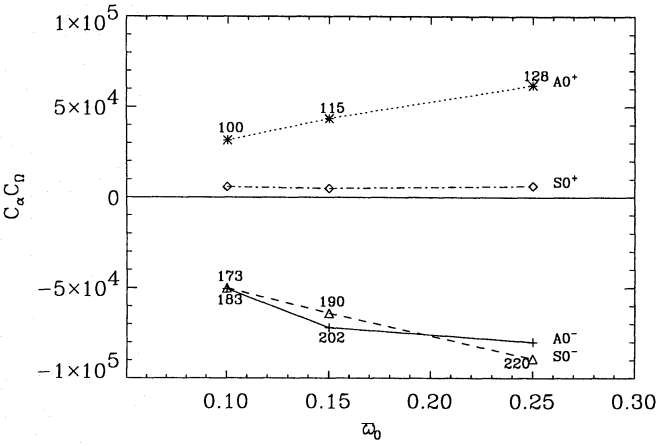

Fig. 2. The critical dynamo numbers for disks with $z_0 = 0.2$ and $\eta_{\rm out}/\eta_{\rm disk} = 20$ as a function of ϖ_0. The numbers next to the data points give the angular frequencies multiplied by ϖ_0 for oscillating modes. Note that it is slightly easier to excite the $S0^-$-mode than the $A0^-$-mode for $\varpi_0 = 0.1$

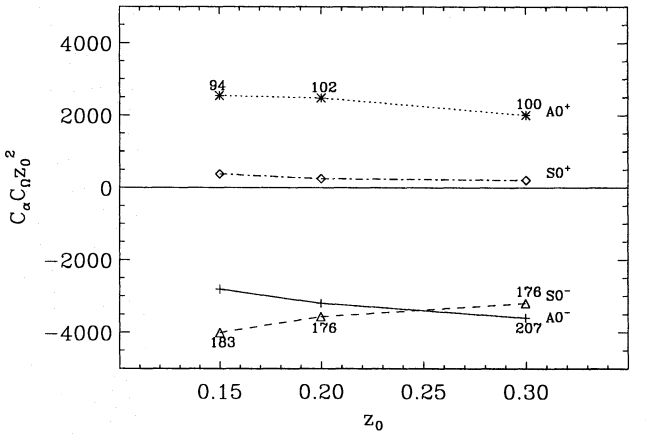

Fig. 3. The critical dynamo numbers for disks with $\varpi_0 = 0.25$ and $\eta_{\rm out}/\eta_{\rm disk} = 20$ as a function of z_0. $C_\alpha C_\Omega$ has been multiplied by z_0^2 to emphasise the behaviour of the $S0^-$- and $A0^-$-modes. The numbers next to the data points give the angular frequencies multiplied by z_0 for oscillating modes

Nonoscillatory magnetic field configurations are always obtained for positive parity when $C_\alpha C_\Omega > 0$, and sometimes for dipolar fields when $C_\alpha C_\Omega < 0$. Apart from the fact that the field pattern is flatter for smaller values of z_0 there are no other significant differences in the resulting field geometry that depend on z_0.

There is a clear difference in the distribution of the magnetic torque for the oscillating dipole mode and the steady quadrupole mode. The distribution of the torque is simple with a strong concentration of negative torque to the inner parts of the disk for the steady quadrupole mode. For the oscillatory dipole mode the

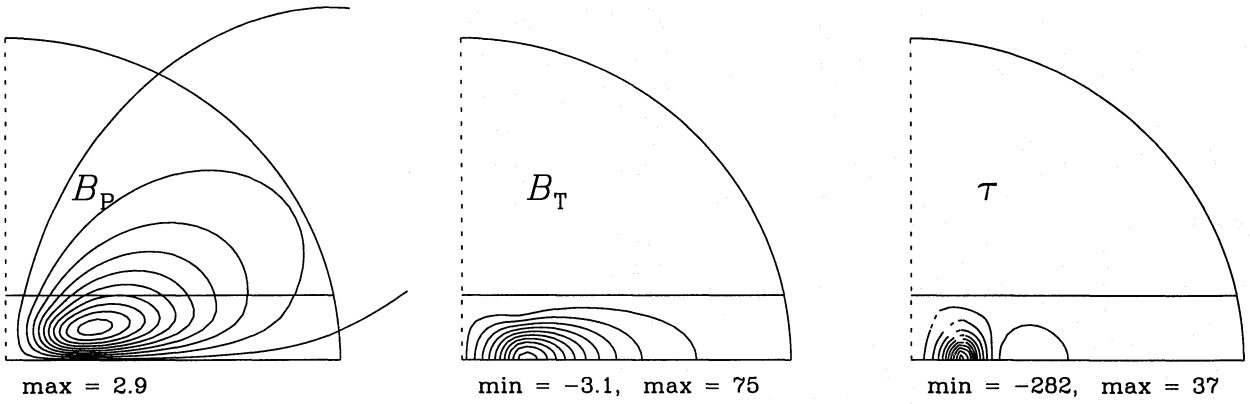

Fig. 4. The most easily excited mode, S0$^+$ (steady), for a flat accretion disk with $\varpi_0 = 0.15$ and $z_0 = 0.2$; Model 0 in Table 4. To the left is shown the poloidal magnetic field, in the middle the toroidal field, and to the right the magnetic torque

Table 3. Critical dynamo numbers for disks with uniform thickness $z_0 = 0.2$, $\eta_{\rm out}/\eta_{\rm disk} = 20$, and $\varpi_0 = 0.25$

	C_Ω	$C_\alpha C_\Omega$	ω
S0	2 000	**6 300**	steady
A0	2 000	62 000	510
S0	2 000	−89 000	880
A0	2 000	**−80 000**	steady
S0	20 000	**6 300**	steady
A0	20 000	69 000	560
S0	20 000	**−120 000**	1 100
A0	20 000	−150 000	steady

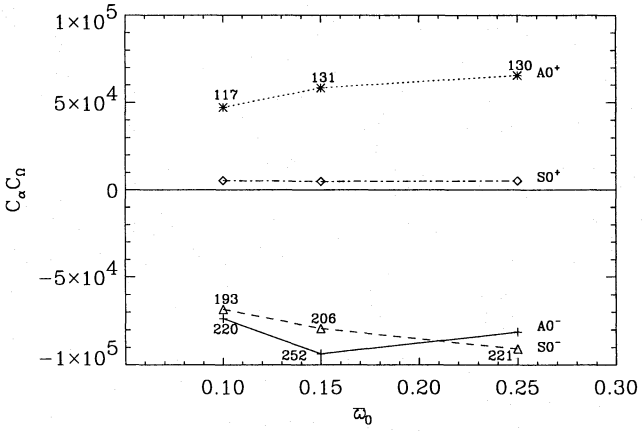

Fig. 5. The critical dynamo numbers for a flared disk with $\zeta = \zeta_0 = 0.15$ and $\eta_{\rm out}/\eta_{\rm disk} = 20$ as a function of ϖ_0. The numbers next to the data points give the angular frequencies multiplied by ϖ_0 for oscillating modes. $\varpi_0 = 0.15$ corresponds to Model a in Table 4

torque has a complicated distribution with alternating regions of positive and negative torques.

It appears that a quadrupolar field is more efficient in promoting accretion. This is in partial agreement with the calculations by Rüdiger et al. (1993) for galactic dynamos. They find accretion in quadrupolar fields, but mostly excretion in dipolar ones, except for weak accretion in a small region in the outer part of the disk. Our finding of locally accreting regions in a dipolar field is not necessarily in contradiction with their results, because different measures for the torque have been employed. Whereas we use a vector relation to calculate the local torque at every grid point, Rüdiger et al. employ a vertical average of $B_r B_\phi$. A more rigorous conclusion concerning accretion in a dipolar field would require a realistic model for the vertical stratification of the disk and the simultaneous solution of the induction and momentum equations.

From the test calculations presented above we conclude that there is good quantitative agreement with the results of SL88, and also qualitative agreement with SL90. The steady A0 solution for $C_\alpha C_\Omega < 0$ changes to an oscillatory mode for small ϖ_0, which is in agreement with SL90.

4. Effects of the geometrical distribution of α and $\eta_{\rm disk}$

4.1. The significance of the geometrical thickness of the disk

To investigate the importance of the thickness of the disk we take the disk model from SL88, but decrease ζ_0 and ζ to 0.15. It turns out that the properties of the dynamo now become similar to those of flat disks. The critical dynamo numbers are given as Model a in Table 4 for $\varpi_0 = 0.15$. For comparison the corresponding dynamo numbers for a flat disk with $\varpi_0 = 0.15$ and $z_0 = 0.2$ are presented as Model 0. To check the influence of the inner rigidly rotating region we calculated the critical dynamo numbers for disks with different ϖ_0. We had to decrease the timestep to $2.5\,10^{-6}$ and $1.25\,10^{-6}$ for $\varpi_0 = 0.15$ and 0.1, respectively. These results are presented in Fig. 5. Note that

Table 4. Critical dynamo numbers for disks with different geometrical properties; see text. The numbers given in parenthesis are the angular frequencies. The three last columns describe the variation of $\eta_{\rm disk}$ with position in the disk, and the geometrical shape of the disk. $\varpi_0 = 0.15$. $z_0 = 0.2$ (for flat disks) or $\zeta = \zeta_0 = 0.15$ (for flared disks)

	$S0^+$		$A0^+$		$S0^-$		$A0^-$		$\eta_{\rm disk}$	geometry	
0	**5 000**	(steady)	44 000	(760)	**−64 000**	(1 300)	−72 000	(1 300)	const.	flat	no cavity
a	**4 800**	(steady)	58 000	(870)	**−79 000**	(1 400)	−94 000	(1 700)	const.	flared	no cavity
b	**7 400**	(steady)	110 000	(1 100)	**−150 000**	(1 900)	**−150 000**	(1 800)	const.	flared	cavity
c	**9 600**	(steady)	99 000	(1 100)	−140 000	(1 900)	**−130 000**	(1 900)	const.	flat	cavity
d	**27 000**	(steady)	290 000	(450)	**−510 000**	(2 300)	−560 000	(2 600)	$\propto z_0^2\Omega$	flared	cavity
e	**3 100**	(steady)	24 000	(1 200)	−32 000	(950)	**−31 000**	(1 900)	$\propto \varpi^{1/2}$	flat	cavity

the general behaviour is similar to that for disks with uniform thickness.

4.2. A gap between the disk and the central object

In several types of objects the disk will not extend down to the compact object. This is the case for instance when the central object is a black hole. Then the inner radius of the disk will coincide with the marginally stable orbit at $3R_{\rm S}$, where $R_{\rm S}$ is the Schwarzschild radius, which determines the location of the event horizon. From an electromagnetic point of view the horizon can be considered as a conductor with a certain resistance (Thorne et al. 1986), and in the following we approximate it with a perfect conductor at $R_{\rm S} = 1$.

The inner radius of the disk is included by multiplying Eq. (9) and the second term in Eq. (10) by a factor $\Theta(\varpi_0 - \varpi)$ where $\varpi_0 = 3R_{\rm S}$. Apart from these modifications relativistic effects are, however, neglected. We study two models with a central cavity: a flared disk with $\varpi_0 = \zeta_0 = \zeta = 0.15$, and a flat disk with $\varpi_0 = 0.15$ and $z_0 = 0.2$, which correspond to Models b and c in Table 4. In those cases the event horizon is represented by the inner border of the grid, which is a perfect conductor at $r = 0.05$. The volume between the inner edge of the disk and the event horizon is assumed to behave as a vacuum. For these calculations we use a timestep of $2.5\,10^{-6}$. The most easily excited dynamo mode for $C_\alpha > 0$ is displayed in Fig. 6.

4.3. The influence of the distribution of the magnetic diffusivity

Lacking a detailed knowledge of the magnetohydrodynamic properties of an accretion disk it is reasonable to assume a constant turbulent magnetic Prandtl number in the accretion disk, and then the magnetic diffusivity will be proportional to the turbulent viscosity, which is assumed to obey the prescription by Shakura & Sunyaev (1973). In this way we get

$$\eta_{\rm disk} = {\rm Pr}_{\rm M}^{-1}\alpha_{\rm SS} z_0^2 \Omega, \tag{13}$$

where $\rm Pr_M$ is the magnetic Prandtl number. We employ this prescription directly for our flared disks setting $\eta_{\rm out}/\eta_{\rm disk}$ to 20 at the outer border, but note that for a more realistic disk z_0 is roughly proportional to ϖ. Due to the limited grid resolution we were unable to simulate a disk that would be both sufficiently thin and have the correct slope. In general we should make $\eta_{\rm disk}$ approximately proportional to $\varpi^{1/2}$. We tested such a dependence of $\eta_{\rm disk}$, but using still the same flat disk geometry. This prescription of $\eta_{\rm disk}$ was normalised such that $\eta_{\rm out}/\eta_{\rm disk} = 10$ at the outer boundary.

The results of these calculations are presented in Table 4 as Models d and e. Typical magnetic fields and torques for the most easily excited modes are presented in Figs. 7 and 8. Comparing Figs. 6 and 7, it is evident that the magnetic field is more evenly distributed in Fig. 7. Because the magnetic diffusivity is now higher in the innermost part of the disk, the dynamo becomes less efficient there. The opposite effect is demonstrated in Fig. 8, where the diffusivity is smallest in the inner part of the disk. The magnetic field and the torque are now more strongly concentrated to the inner part of the disk.

5. Nonlinear dynamos

There are several ways in which nonlinear effects are important and modify the linear results presented above. On the global scale the magnetic field will affect the motion of the plasma leading to deviations from the imposed velocity field. Such effects can be handled by simultaneously solving the induction and Navier-Stokes equations. This is a major undertaking and will not be considered here. In a simplified form such a model was presented by Campbell (1992). He obtains eigensolutions of the height averaged, time independent magnetohydrodynamic equations.

The magnetic field can modify the turbulence and decrease the efficiency of the α-effect. This phenomenon is customarily described by the so-called α-quenching. Another important effect is magnetic buoyancy. Because the magnetic field contributes to the total pressure, a region with a strong magnetic field will be less dense than the surroundings and become buoyant. Magnetic buoyancy will lead to a transport of magnetic flux along the direction of the effective gravity, i.e. in the vertical direction.

The aim of this section is to provide a few examples of nonlinear effects in accretion disks. We will defer a comprehensive survey of nonlinear disk dynamos to a future paper.

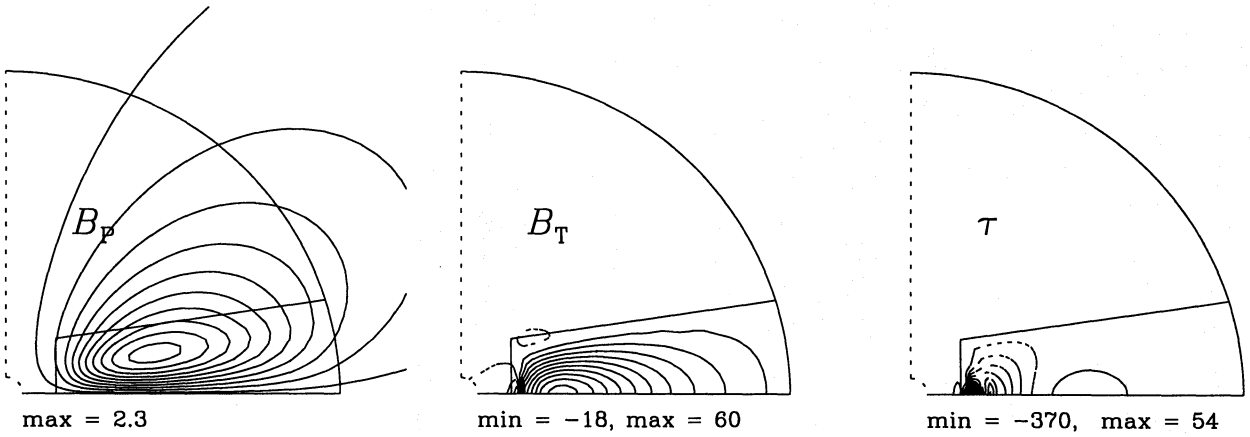

Fig. 6. The most easily excited dynamo mode, S0$^+$ (steady), for a flared disk with $\zeta = \zeta_0 = 0.15$ and an inner edge at $\varpi = 0.15$; Model b in Table 4. The inner border of the grid is located at $r = 0.05$ and is a perfect conductor. $\eta_{\rm out}/\eta_{\rm disk} = 20$

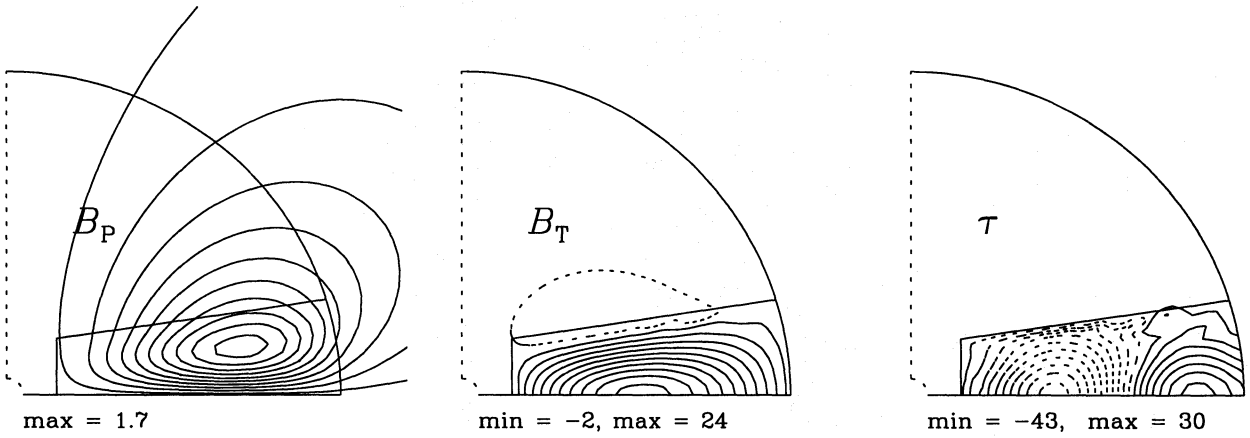

Fig. 7. The most easily excited dynamo mode, S0$^+$ (steady), for a truncated flared disk with $\varpi_0 = \zeta = \zeta_0 = 0.15$; Model d in Table 4. The magnetic diffusivity goes as $z_0^2\Omega$ and is normalised such that $\eta_{\rm out}/\eta_{\rm disk} = 20$ at the outer boundary

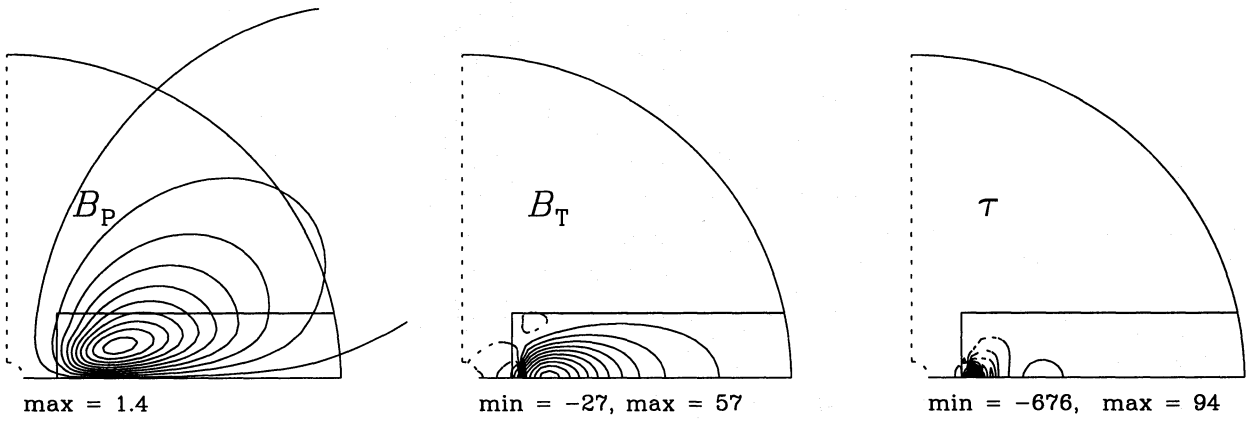

Fig. 8. The most easily excited dynamo mode, S0$^+$ (steady), for a flat disk with $\varpi_0 = 0.15$, $z_0 = 0.2$; Model e in Table 4. The magnetic diffusivity goes as $\varpi^{1/2}$ and is normalised such that $\eta_{\rm out}/\eta_{\rm disk} = 10$ at the outer boundary

Table 5. Parameters used as input for nonlinear disk dynamos and the resulting maximal energy, parity and angular frequency. For flaring and flat disks $\zeta = \zeta_0$ and z, respectively, are given. For Models 3 $\eta_{\rm disk}$ is given by Eq. (13), and for Models 4 and 5 $\eta_{\rm disk}$ is proportional to $\varpi^{1/2}$. Models 1-4 include α-quenching and Models 5 magnetic buoyancy. An asterisk indicates that α_B or γ_B is a function of ϖ.

Model	ϖ_0	ζ_0	z_0	$\eta_{\rm disk}(R)$	C_Ω	C_α	α_B	γ_B	lg $E_{\rm max}$	P	ω
1a	0.15	0.15	–	0.05	1 000 000	+400	$1.8\,10^{-6}$	0	13.62	0.94	0
1b	0.15	0.15	–	0.05	1 000 000	−400	$1.8\,10^{-6}$	0	12.11	−0.92..0.92	(irreg.)
2a	0.15	0.15	–	0.05	1 000 000	+400	$1.8\,10^{-6}$	0	13.66	0.93	0
2b	0.15	0.15	–	0.05	1 000 000	−400	$1.8\,10^{-6}$	0	12.01	−0.92..0.91	(irreg.)
3a	0.15	0.15	–	0.05	1 000 000	+400	$1.8\,10^{-6}$	0	13.09	0.95	0
3b	0.15	0.15	–	0.05	1 000 000	−400	$1.8\,10^{-6}$	0	11.77	−0.91..0.92	(irreg.)
4a	0.15	–	0.2	0.1	250 000	+200	$1.8\,10^{-6}$	0	11.82	0.91	0
4b	0.15	–	0.2	0.1	250 000	−200	$1.8\,10^{-6}$	0	10.53	−0.80..0.90	(irreg.)
4c	0.15	–	0.2	0.1	250 000	+200	$1.8\,10^{-6}$ *	0	13.78	0.98	0
4d	0.15	–	0.2	0.1	250 000	−200	$1.8\,10^{-6}$ *	0	11.68	−0.83..0.95	(irreg.)
5a	0.15	–	0.2	0.1	1 000	+6	0	$3\,10^{-5}$	7.51	1	0
5b	0.15	–	0.2	0.1	1 000	−60	0	$3\,10^{-5}$	5.31	1	1 900
5c	0.15	–	0.2	0.1	1 000	+6	0	$3\,10^{-5}$ *	8.94	1	0
5d	0.15	–	0.2	0.1	1 000	−60	0	$3\,10^{-5}$ *	7.21	1	2 000

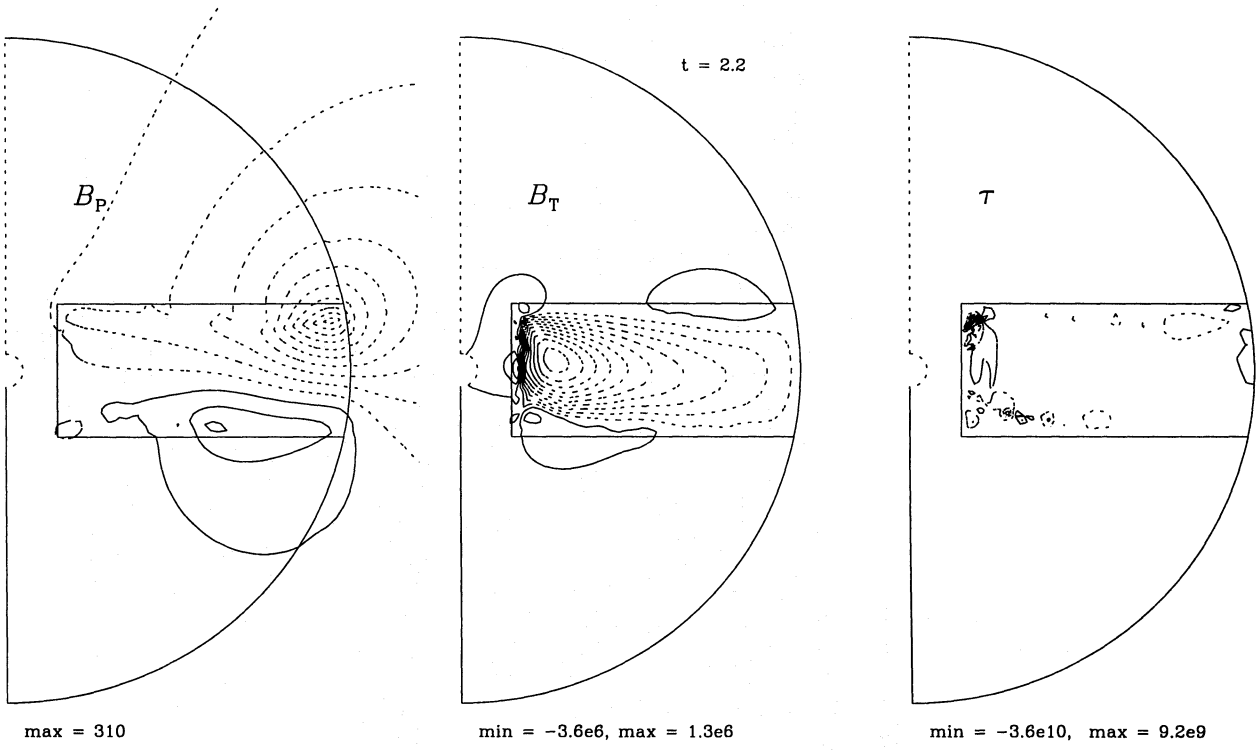

Fig. 9. Nonlinear dynamo solution for a disk of uniform thickness with $\varpi_0 = 0.15$, $z_0 = 0.2$. The magnetic diffusivity goes as $\varpi^{1/2}$, $\eta_{\rm out}/\eta_{\rm disk} = 10$. $C_\Omega = 250\,000$, $C_\alpha = 200$ and $\alpha_B = 1.8\,10^{-6}$ (Model 4a)

5.1. α-quenching

In general α-quenching is an anisotropic effect, but the theoretical expressions are fairly complicated (e.g. Rüdiger & Kichatinov 1993) and not yet well established. Therefore, in order to keep our model simple, we assume here an isotropic α-quenching. It is often taken in the form

$$\alpha = \frac{\alpha_0}{1 + \alpha_B \boldsymbol{B}^2}, \tag{14}$$

where α_B is a measure of the strength of the α-quenching. α_B can be estimated by assuming that quenching becomes important when the magnetic energy density becomes comparable

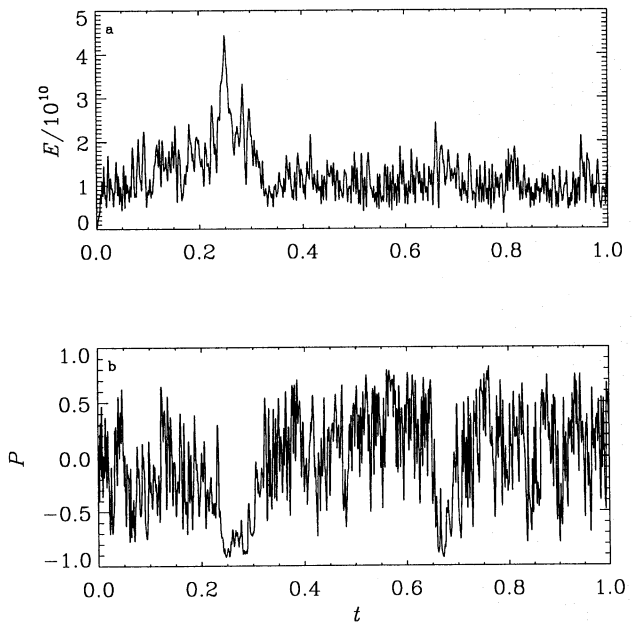

Fig. 10. a: The magnetic energy as a function of time for a dynamo with α-quenching, $\alpha_B = 1.8\,10^{-6}$, $C_\alpha = -200$ and $C_\Omega = 250\,000$ in a disk of uniform thickness $z_0 = 0.2$ with its inner edge at $\varpi_0 = 0.15$. The diffusivity in the disk is proportional to $\varpi^{1/2}$ with $\eta_{\rm out}/\eta_{\rm disk} = 20$. **b**: Parity P as a function of time for the same disk dynamo

with the kinetic energy density of the turbulence, that is we put $\alpha_B = 1/\boldsymbol{B}^2_{\rm eq}$ in dimensional units, where $\boldsymbol{B}^2_{\rm eq} = \mu_0\rho u_{\rm t}^2$, and $u_{\rm t}$ is the rms-velocity of the turbulence. Using again $(\mu_0\rho_0)^{1/2}\eta_{\rm disk}(R)/R$ as the unit for the magnetic field together with Eq. (13) evaluated at R for $\eta_{\rm disk}(R)$, this gives

$$\alpha_B = \frac{\mu_0\rho_0\left(\eta_{\rm disk}(R)/R\right)^2}{\boldsymbol{B}^2_{\rm eq}} = \frac{\alpha_{\rm SS}^2\xi^2(R)}{{\rm Ma}^2{\rm Pr}_{\rm M}^2}\left(\frac{p}{p_0}\right)^{-1}, \qquad (15)$$

where $\xi(R) = z_0(R)/R$, Ma is the Mach number for the turbulence, p the pressure and p_0 denotes the pressure at $\varpi = R$. Ma is expected to be of the same order of magnitude as $\alpha_{\rm SS}$.

This α-quenching was introduced in several of our disk models, both flat and flared. For all these disk models we used $\varpi_0 = 0.15$ and a timestep of $1.25\,10^{-6}$. For the flat disks $z_0 = 0.2$ and for the flared ones $z_0 = 0.15$. The calculations were performed on a 41×81 grid covering the two quadrants in the meridional plane, so that we were not forced to impose a specific parity on the magnetic field. The initial magnetic field was prescribed randomly and was not of a specific parity. The parameters were chosen to roughly represent the accretion disk around a stellar mass black hole. Unless otherwise stated we have assumed a constant α_B. The models are described in detail in Table 5. Model 1 is a flared disk (with constant $\eta_{\rm disk}$) extending from the z-axis to the outer border of the grid with the thickness increasing linearly from 0.15 on the axis with a slope of 0.15. Model 2 is the same flared disk, but the central part inside $\varpi = 0.15$ has been replaced by a vacuum. Model 3 is also a truncated flared disk, but $\eta_{\rm disk}$ inside the disk is described by Eq. (13) normalised as previously. Finally Model 4 is a truncated flat disk similar to the one in Sect. 4.3. By mistake the dynamo numbers for Model 4 were set to smaller values than for the other models, but as Model 4 seemed to be more stable than the other ones, it was decided not to recalculate it. Model 4 c and d are similar to a and b, except that α_B is proportional to ϖ^3 and normalised to $1.8\,10^{-6}$ at $\varpi = 1$. From thin disk theory we do not expect α_B to be able to vary more rapidly than this.

Results of the simulations are presented in Table 5. $E_{\rm max}$ denotes the maximal magnetic energy, and P is a continuous measure of the parity of the field,

$$P = \frac{E^{(\rm S)} - E^{(\rm A)}}{E^{(\rm S)} + E^{(\rm A)}} \qquad (16)$$

(Brandenburg et al. 1989), where $E^{(\rm A)}$ and $E^{(\rm S)}$ are the energies of the antisymmetric and symmetric parts of the magnetic field. In the cases with $C_\alpha > 0$ the solution tends to settle to a definite value of P, which is given in Table 5. However in the cases with $C_\alpha < 0$ the solution kept oscillating rapidly and irregularly in both P and $\lg E$. In those cases the interval covered by P is given instead. An interesting behaviour appeared in Models 1a and 2a. The solutions seem to converge to specific values of E and P, but suddenly both P and E drop to considerably smaller values. After a short while, on the order of a tenth of the diffusion time scale, the solution returned to almost the old position or slightly above it. This could mean that the model had not yet reached a steady state, which may be one of much lower P. To investigate this hypothesis, Model 1a was recalculated starting from a seed field with $P \approx -1$. In this case the solution still evolved towards the same field configuration with P only slightly smaller than +1.

Some general features of the nonlinear simulations can be mentioned. A plot of the field of a dynamo with $C_\alpha > 0$ is displayed in Fig. 9. The general field structure is practically independent of the disk model and the structure is roughly the same as in the linear calculations, but the field is somewhat more evenly distributed within the disk. The mainly quadrupolar field has a small dipolar component also, i.e. the parity of the magnetic field is mixed. All nonoscillatory mixed parity solutions known so far show a slow change in P, and we cannot rule out that the same also happens here. The poloidal field has its maximum in the outer part of the disk, which is explained by the dynamo being more strongly quenched in the inner part of the disk, where the toroidal field is strong due to the rapid winding up of the field lines.

For $C_\alpha < 0$ the field is much more complicated, and appears to vary chaotically on short time scales. Often the magnetic field appears to vary on length scales smaller than the half thickness of the disk, which is assumed to be the relevant mixing length. This is somewhat worrying, because there are limitations to the length and time scales, which can be handled by our numerical code and mean-field theory. Further mean-field theory is not able to describe variations in the mean field on length scales smaller than the mixing length.

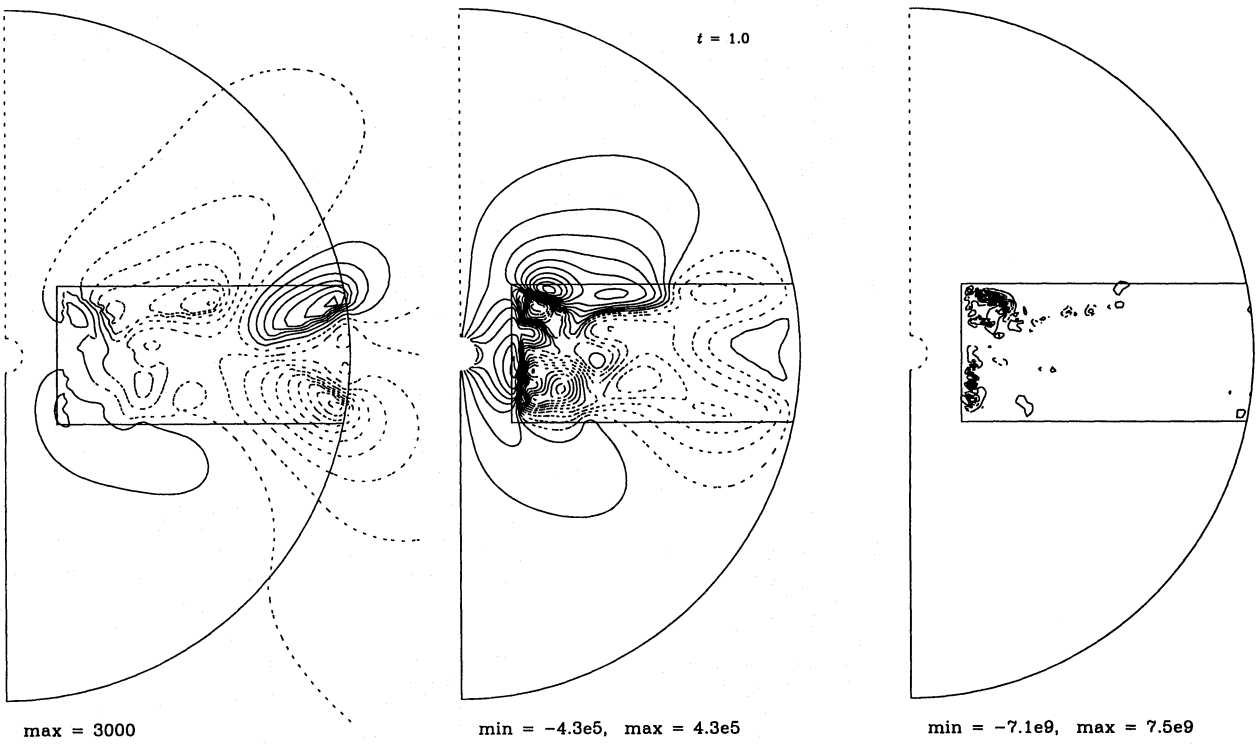

Fig. 11. Nonlinear dynamo for a disk of uniform thickness with $\varpi_0 = 0.15$, $z_0 = 0.2$. The magnetic diffusivity goes as $\varpi^{1/2}$, $\eta_{\rm out}/\eta_{\rm disk} = 10$. $C_\Omega = 250\,000$, $C_\alpha = -200$ and $\alpha_B = 1.8\,10^{-6}$ (Model 4b)

To investigate the reality of the chaotic solutions, Model 4b was recalculated with 63×127 grid points and a timestep of $8\,10^{-7}$. The new solution was chaotic too, with P varying between -0.92 and 0.82, and $\lg E_{\rm max} = 10.38$. Thus it seems safe to conclude that the numerical code provides a truthful representation of the solution. To illustrate the irregular behaviour of the dynamo mode we plot E and P as functions of time for the run with higher resolution in Fig. 10. We also present a snapshot of the magnetic field in Fig. 11.

In Models 4c and d we also studied the effects of using a variable α_B. Because of the strong ϖ-dependence, α_B is small in the inner part of the accretion disk, and thus both the toroidal and poloidal field attain their maxima in the inner part of the disk, so that the field distribution is in a sense more similar to the linear case. The total magnetic energy will increase because the quenching is effectively reduced. Apart from this we do not find any significant changes caused by a ϖ-dependence of α_B.

5.2. Magnetic buoyancy

It is expected that buoyancy instabilities are important in accretion disks (e.g. Galeev et al. 1979, Sakimoto & Coroniti 1989). Buoyancy instabilities lead to a transport of magnetic flux against the direction of effective gravity, i.e. roughly in the vertical direction. Such a transport can formally be represented by a velocity term in the induction equation. According to Moss et al. (1990) this velocity can be expressed as

$$\boldsymbol{u}_B = \gamma_B \boldsymbol{B}^2 \hat{\boldsymbol{z}}, \tag{17}$$

where γ_B is a parameter describing the strength of the buoyancy. A nonvanishing drift velocity u_B exists only if there is a density difference $\Delta\rho$ between the upwards motions of buoyant material and the associated return flow. Otherwise the return flow would compensate for the upflow and there would be no net effect. Furthermore, the drift velocity is proportional to the surface fraction k covered by the upwards motions times the typical rms-velocity u_t, i.e.

$$u_B \approx k u_t \frac{\Delta\rho}{\rho} \approx \tfrac{1}{2} k u_t \frac{v_A^2}{c_s^2}. \tag{18}$$

In dimensionless units we find for γ_B

$$\gamma_B = \frac{u_B/[u]}{\boldsymbol{B}^2/[B]^2} \approx \tfrac{1}{2} k \mathrm{Ma}\, \mathrm{Pr}_M^{-1} \alpha_{\rm SS} \xi(R) \left(\frac{p\rho}{p_0\rho_0}\right)^{-1/2}. \tag{19}$$

It is evident from the results for α-quenching that the exact geometrical shape of the disk is not significant for the dynamo. Thus all our calculations were done with Model 4 in the preceding section. We decided to take $\xi = 0.01$, a reasonable value for an accretion disk, $\mathrm{Pr_M} = 1$, and $\mathrm{Ma} = \alpha_{\rm SS} = 0.1$, a value used in Sect. 2.2. This gives $\gamma_B = 3\,10^{-5}$. Because initial experiments suggested that it would be difficult to treat realistic

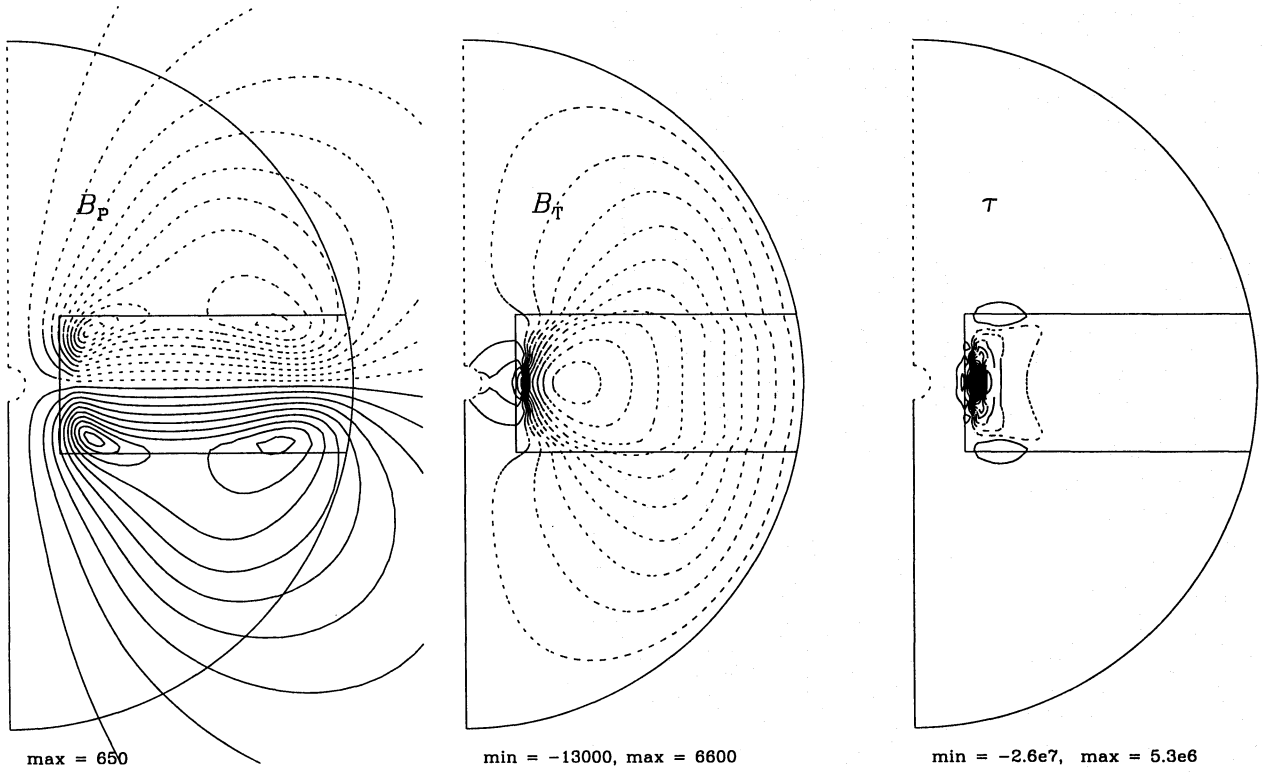

Fig. 12. The S0$^+$ solution for a dynamo with buoyancy in a disk with $z_0 = 0.2$, $\varpi_0 = 0.15$. The magnetic diffusivity goes as $\varpi^{1/2}$, with $\eta_{\rm out}/\eta_{\rm disk} = 10$ at the outer boundary. $C_\Omega = 1\,000$, $C_\alpha = 6$, and $\gamma_B = 3\,10^{-5}$ (Model 5a)

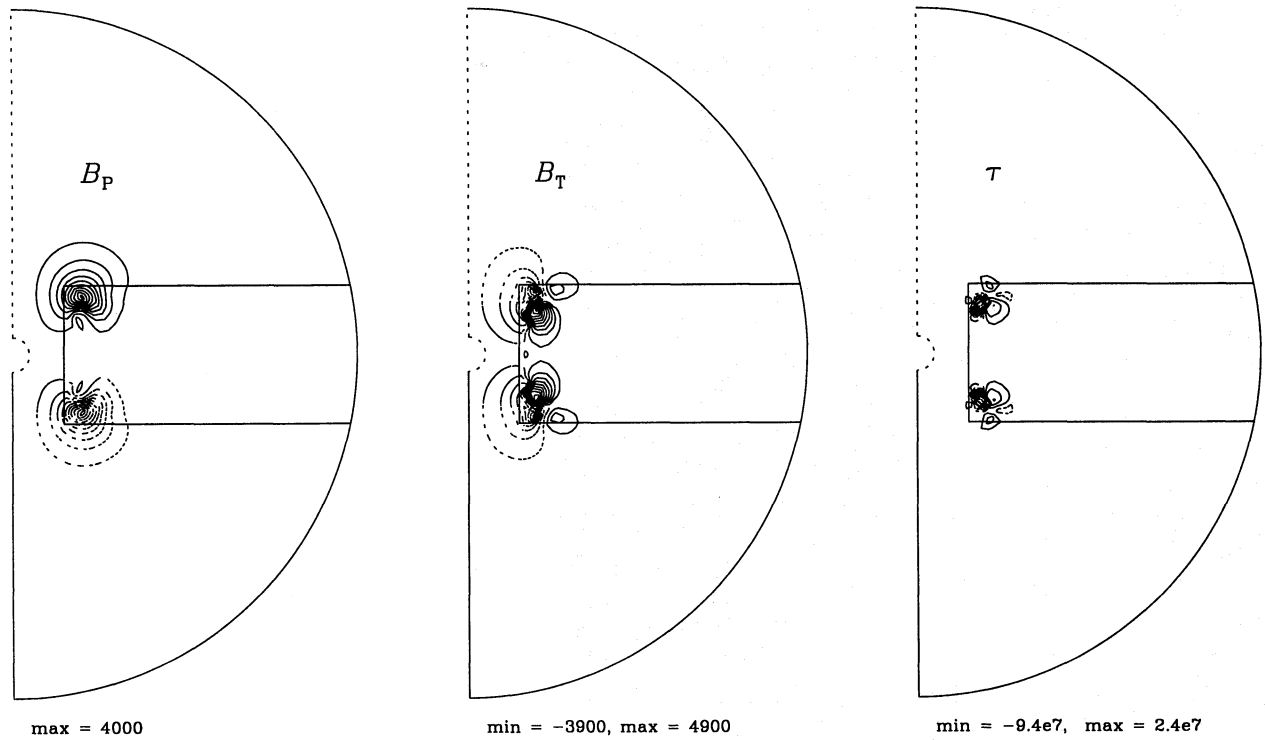

Fig. 13. The S0$^-$ solution for a dynamo with buoyancy in a disk with $z_0 = 0.2$, $\varpi_0 = 0.15$. The magnetic diffusivity goes as $\varpi^{1/2}$, with $\eta_{\rm out}/\eta_{\rm disk} = 10$ at the outer boundary. $C_\Omega = 1\,000$, $C_\alpha = -60$, and $\gamma_B = 3\,10^{-5}$ (Model 5b)

values of γ_B and the dynamo numbers simultaneously, we took dynamo numbers that were roughly twice the critical values, i.e. $C_\alpha = -60$, and $C_\alpha = 6$, respectively, and in both cases $C_\Omega = 1\,000$. The most essential parameters and results for these models are presented as Model 5 in Table 5. Models 5a and b are calculated with a constant γ_B, whereas Models 5c and d assumes that $\gamma_B \propto \varpi^2$, which is roughly what is expected for a thin accretion disk, and then γ_B is normalised to its tabular value at $\varpi = R$. We first discuss models with a constant γ_B.

For positive dynamo numbers the general behaviour is similar to the linear case, that is the solution is quadrupolar and steady, but a considerable amount of toroidal flux is present in the surroundings of the disk (Fig. 12). This is caused by the buoyancy effect and is only possible when the diffusivity is still finite in the surrounding medium. An interesting detail is that the magnetic field grows at a steady rate initially, but then the field grows much more rapidly for a short time before the dynamo saturates. This later increase in growth rate is caused by the onset of magnetic buoyancy. The magnetic buoyancy transports the magnetic field from the equator to regions with a stronger α-effect, where the magnetic field is subsequently amplified (cf. Brandenburg et al. 1993).

More dramatical changes are found for a negative C_α. The solution is oscillatory in both energy and parity, but the oscillation in parity is damped and tends to approach $P = 1$. The field structure is displayed in Fig. 13. Note that the dynamo action is concentrated to two regions at the inner edge of the disk, close to the upper and lower surfaces of the disk.

We did not find any significant qualitative changes when we introduced a ϖ-dependent γ_B. The main difference is an increase in the magnetic energy, because γ_B is effectively decreased.

6. Discussion

Many accretion disks can be described satisfactorily by the theory of thin accretion disks. Such disks are much thinner and have a much larger radial extent than what we can reproduce in our model. This is true in particular for accretion disks in protostellar objects and active galactic nuclei, where the size of the disk is not determined by the size of the binary. Of course there are also theoretical models for thick accretion disks (e.g. Abramowicz et al. 1980), but the disk shape that we employed does not resemble a thick disk. One might argue that we have simulated only the innermost part of a thin disk, but then it becomes questionable to assume vacuum boundary conditions at the outer border of the grid.

The aim of this paper has not been to model the magnetic field of a real accretion disk, but merely to demonstrate in an approximate manner the viability of dynamo action in an accretion disk, and to provide a few guidelines to the qualitative behaviour of a disk dynamo. We find that the strongest fields will build up where the gradient of the angular velocity is the strongest, which will always be in the innermost part of the disk, and we expect that this part of the field will be only weakly affected by the outer boundary conditions. Thus, our models can be applied to those regions where the magnetic field strength attains its maximum, but we are unable to make any predictions about the magnetic field further out in the accretion disk corresponding, for instance, to where the carbonaceous chondrites formed in the solar nebula (Levy 1978).

6.1. Turbulence and the α-effect

In this paper we have assumed the simplest form of the α-effect, that is isotropic and so affects the magnetic field to the same degree in all directions. There are calculations hinting at an anisotropic α-effect. For example Vishniac et al. (1990) and Vishniac & Diamond (1992) found strong anisotropies in the case where the α-effect is caused by internal waves. Rüdiger (1990) found another type of anisotropy in the case of turbulence in a galactic disk. The α-effect normally results in a positive value for C_α, although exceptions are conceivable. From the presented simulations it is clear that the dynamo will change character completely if $C_\alpha < 0$. It is also worth mentioning the phenomenological disk dynamo presented by Tout & Pringle (1992), that employs different physical mechanisms for generating the three components of the magnetic field. The Balbus-Hawley instability (Balbus & Hawley 1991) generates the radial field, buoyancy is the source of the vertical field, and shearing motion produces the toroidal field. Such a model is intrinsically anisotropic. Thus it may be possible that the detailed behaviour of magnetohydrodynamic turbulence in accretion disks may change the character of the dynamo, and farther study of this problem is therefore essential.

6.2. Angular momentum transport

It is widely believed that some unknown type of turbulent viscosity is responsible for the transport of angular momentum in accretion disks, but so far no model of this turbulence has gained widespread acceptance. The main problem appears to be that this viscosity is assumed to be due to a microscopic hydrodynamic or magnetohydrodynamic process, which is difficult to model in a realistic way. On the other hand some authors have suggested that macroscopic processes may be responsible for the angular momentum transport, e.g. spiral density waves, and magnetohydrodynamic outflows exerting a torque on the disk (e.g. Blandford & Payne 1982).

Stepinski & Levy (1990a) calculated the torque that a dipolar magnetic field generated by a mean-field dynamo would exert on a disk and concluded that it would be able to transport the angular momentum outwards. In this paper we have calculated the torque in the same way as Stepinski & Levy, but we have extended the calculations to include quadrupolar dynamo solutions and solutions of mixed parity. In general we find a stronger negative torque in a quadrupolar field. Rüdiger et al. (1993) have found a similar effect for a magnetic field of even parity in a galactic disk. For a dipolar magnetic field it is more complicated. From our numerical simulations it is clear that such a field will generate regions with both positive and nega-

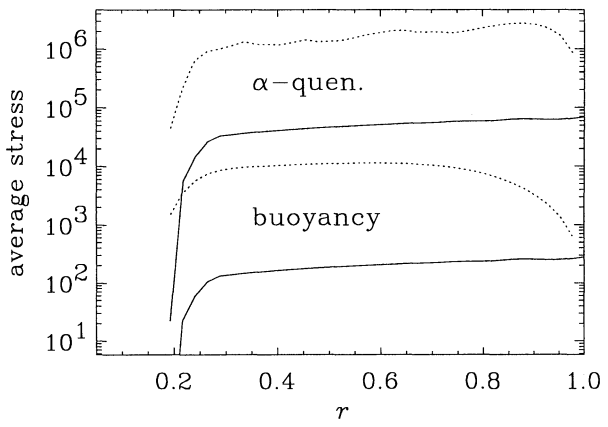

Fig. 14. Vertical averages of the r,ϕ-components of the magnetic and viscous stress tensors (dotted and solid lines, respectively) for Model 4a (α-quenching) and Model 5a (magnetic buoyancy)

tive torques, whereas Rüdiger et al. (1993) found that a dipolar field would mainly achieve excretion in a galactic disk.

It is of considerable interest to compare the viscous and magnetic torques acting in the accretion disk. Because of the oversimplified nature of our disk model it is difficult to do this with any certainty, but a few general trends can be found. A simple way to estimate the importance of the magnetic torque is to compare vertical averages of the r,ϕ-components of the magnetic and viscous stress tensors. Assuming $\mathrm{Pr_M} = 1$, we find that for Model 4a (5a) this ratio is around 30 (100), i.e. magnetic fields would indeed be responsible for driving the accretion (Fig. 14). (We were unable to attain realistic dynamo numbers for Model 5a, which causes too small values for the average stress in the case with magnetic buoyancy.) One can also express the magnetic torque in terms of the corresponding α_{SS}. Estimates for $\alpha_{\mathrm{SS}}^{\mathrm{mag}} = \tau/(p\varpi)$ typically lead to values larger than unity, indicating that the magnetic pressure exceeds the ordinary pressure and that magnetic buoyancy will be important. Clearly, this result is model dependent and sensitive to all input parameters. Finally, one should emphasise that we have not included the contribution from the fluctuating magnetic field, which is at least comparable to, or may even exceed, the mean magnetic field (see Pudritz 1981).

6.3. Generation of jets

One of the most popular scenarios for collimated outflows from accretion disks is that they are magnetohydrodynamic winds, which become collimated due to the magnetic field frozen into them (for a review see Blandford 1989). In general these models have assumed a dipole field in the disk. This was also assumed by Yoshizawa & Yokoi (1993) who recently presented a model including both a dynamo and a jet. As is evident from our calculations, accretion disks are more likely to possess quadrupolar fields, or perhaps dipolar fields with structure immensely more complex than the classical dipole field. Some authors (e.g. Wang et al. 1990, 1992) have actually considered generation of jets in quadrupolar fields, or even in fields of mixed parity. It turns out that it is possible to generate magnetohydrodynamic jets even in those cases, but the mechanism is less efficient, and the resulting jets are less energetic than for a dipole field. An interesting possibility is that in some cases the two jets may be of unequal strength. This is often seen in the outflows from active galactic nuclei, and is normally explained as a relativistic beaming effect.

6.4. Magnetically induced variability

The effects of the solar dynamo are most prominently seen in the 11 year sunspot cycle. Based on our results, it is unlikely that a similar mechanism will occur in an accretion disk, as the most easily excited mode is a steady quadrupolar mode. However this does not exclude magnetic variability in an accretion disk, as most of the activity we see on the sun is not connected to the mean-field, but to the fluctuating field, which is only included implicitly in our simulations.

On the other hand it is evident from our simulations that with $C_\alpha < 0$, which is less likely to occur, the mean magnetic field will fluctuate rapidly and irregularly on time scales as short as a hundredth of a diffusion time. Such fluctuations may give rise to observable variability, but we refrain from discussing possible manifestations of this variability because this would require a more detailed knowledge of the interaction between the magnetic field and the disk. Similar types of chaotic behaviour have only recently been found for a two-dimensional dynamo in a torus geometry (Brooke & Moss 1993). The physical significance of such chaotic solutions is somewhat questionable, because the length scale of the mean magnetic field is much smaller than the thickness of the disk. This leads to a problem because in order for mean-field theory to be applicable, the length scale of the mean magnetic field is assumed to be much larger than that of the turbulent motion.

7. Conclusions

With reasonable estimates of the strength of turbulence in an accretion disk, there will be dynamo action in accretion disks leading to the build up of magnetic fields. For a thin disk it is expected that the magnetic field will be quadrupolar, although this conclusion is to some extent dependent upon the properties of the turbulence. The quadrupolar field exerts a torque on the disk and can be able to drive the accretion. In our nonlinear calculations we find two types of behaviour for dynamos with α-quenching depending on the sign of C_α. For $C_\alpha > 0$, the dynamo behaves roughly like in the linear case, but the field deviates slightly from a pure quadrupolar one, i.e. $0.9 < P < 1$. On the other hand for $C_\alpha < 0$ the mean magnetic field fluctuates irregularly in both $\lg E$ and P. Introducing magnetic buoyancy in a model without α-quenching we find that the general behaviour of the dynamo is preserved, but that the distribution of the magnetic field is affected. For $C_\alpha < 0$ the magnetic field is

concentrated in two regions close to the upper and lower surfaces of the disk, where both the differential rotation and the α-effect is strongest. For $C_\alpha > 0$ there is an accumulation of toroidal flux outside the disk. However we believe that the second effect at least to some extent is caused by a too low diffusivity ratio $\eta_{\rm out}/\eta_{\rm disk}$ in our simulations.

Future improvements to our model might include modelling a significantly thinner disk, by either using a nonuniform spherical grid or by working in cylindrical coordinates. Furthermore, because of the close coupling between the magnetic field, the angular momentum transport, and the energy production in accretion disks, it is necessary to take hydrodynamical and thermodynamical effects into account. It must also be stressed that there is no point in performing very elaborate mean-field calculations as long as we do not have a firm understanding of the microscopic turbulent processes working in the accretion disk. It cannot be ordinary convective turbulence, and in many cases convection, if it exists at all, might not carry very much heat (Shakura et al. 1978), but the turbulence might be vigorous and thus important for the dynamo. A possible model for the origin of the turbulence has been suggested by Balbus & Hawley (1991), and Hawley & Balbus (1991, 1992) have presented two-dimensional simulations of the nonlinear evolution (but see Knobloch 1992). Clearly, more work on this topic is needed, both analytical and numerical.

Acknowledgements. We are grateful to David Moss and the referee, Tomasz Stepinski, for useful comments on the paper. UT thanks Nordita (Copenhagen), the Observatory and Astrophysics Laboratory (Helsinki), and the High Altitude Observatory (Boulder), where parts of the work has been carried out, for hospitality. He would also like to thank the Royal Physiographical Society in Lund for a travel grant. The computations presented here have been carried out on the Cray X-MP 4/16 at the National Supercomputer Centre, Linköping, Sweden.

References

Abramowicz, M. A., Calvani, M., Nobili, L., 1980, ApJ, 242, 772
Balbus, S. A., Hawley, J. F., 1991, ApJ 376, 214
Blandford, R. D., 1989, in F. Meyer et al. (eds.), Theory of accretion disks, Kluwer Academic Publishers, Dordrecht, pp 35
Blandford, R. D., Payne, D. G., 1982, MNRAS 199, 883
Brandenburg, A., Krause, F., Meinel, R., Moss, D., Tuominen, I., 1989, A&A 213, 411
Brandenburg, A., Donner, K. J., Moss, D., Shukurov, A., Sokoloff, D. D., Tuominen, I. 1993, A&A 271, 36
Brooke, J. M., Moss, D., 1993, MNRAS submitted
Camenzind, M., 1991, Rev. Mod. Astron. 3, 234
Campbell, C. G., 1992, Geophys. Astrophys. Fluid Dyn. 63, 197
Galeev, A. A., Rosner, R., Vaiana, G. S., 1979, ApJ 229, 318
Hawley, J. F., Balbus, S. A., 1991, ApJ, 376, 223
Hawley, J. F., Balbus, S. A., 1992, ApJ, 400, 595
Horne, K., Saar, S. H., 1991, ApJ 374, L55
Knobloch, E., 1992, MNRAS, 255, 25P
Krause, F., Rädler, K. H., 1980, Mean-Field Magnetohydrodynamics and Dynamo Theory, Pergamon, Oxford
Levy, E. H., 1978, Nat 276, 481
Marsh, T. R., Horne, K., 1990, ApJ 349, 593
Moss, D., Tuominen, I., Brandenburg, A., 1990, A&A 228, 284
Noyes, R. W., Hartmann, L., Baliunas, S. L., Duncan, D. K., Vaughan, A. H., 1984, ApJ 279, 763
Parker, E. N., 1971, ApJ 163, 255
Pudritz, R. E., 1981, MNRAS 195, 881 and 195, 897
Roberts, G.O. 1972, Phil. Trans. Roy. Soc. A271, 411
Rosner, R., DeLuca, E., 1989, in The Center of the Galaxy (ed M. Morris), Kluwer Acad. Publ., Dordrecht, pp 319
Rüdiger, G., 1990, Geophys. Astrophys. Fluid Dyn. 50, 53
Rüdiger, G., Elstner, D., Schultz, M., 1993, A&A 270, 53
Rüdiger, G., Kichatinov, L. L., 1993, A&A 269, 581
Sakimoto, P. J., Coroniti, F. V., 1989, ApJ 342, 49
Shakura, N. I., Sunyaev, R. A., 1973, A&A 24, 337
Shakura, N. I., Sunyaev, R. A., Zilitinkevich, S. S., 1978, A&A, 62, 179
Shields, G. A., Wheeler, J. C., 1976, Ap. Lett. 17, 69
Skumanich, A., 1972, ApJ 171, 565
Soward, A. M., 1992, Geophys. Astrophys. Fluid Dyn., 64, 163, and 64, 201
Stepinski, T. F., 1992, Icarus 97, 130
Stepinski, T. F., Levy, E. H., 1988, ApJ 331, 416, (SL88)
Stepinski, T. F., Levy, E. H., 1990a, ApJ 350, 819
Stepinski, T. F., Levy, E. H., 1990b, ApJ 362, 318, (SL90)
Stepinski, T. F., Levy, E. H., 1991, ApJ 379, 343
Stix, M., 1975, A&A 42, 85
Takahara, F., 1979, Prog. Theor. Phys. 62, 629
Thorne, K. S., Price, R. H., Macdonald, D. A., 1986, Black Holes: The Membrane Paradigm, Yale University Press, New Haven, London
Tout, C. A., Pringle, J. E., 1992, MNRAS 259, 604
Vishniac, E. T., Diamond, P., 1992, ApJ 398, 561
Vishniac, E. T., Jin, L., Diamond, P., 1990, ApJ 365, 648
Wang, J. C. L., Sulkanen, M. E., Lovelace, R. V. E., 1990, ApJ 355, 38
Wang, J, C. L., Sulkanen, M. E., Lovelace, R. V. E., 1992, ApJ 390, 46
Yoshizawa, A., Yokoi, N., 1993, ApJ, 407, 540

This article was processed by the author using Springer-Verlag LaTeX A&A style file version 3.